ACS APPLIED BIO MATERIALS

www.acsabm.org Article

Improved Graphitization of Lignin by Templating Using Graphene Oxide Additives

Sandra N. Ike* and Randy L. Vander Wal

Cite This: ACS Appl. Bio Mater. 2024, 7, 8319−8327 Read Online

ACCESS | Metrics & More | Article Recommendations

ABSTRACT: Techniques to improve the graphitization of lignin, the second most abundant natural polymer, are in great demand as a viable means to obtain cost-effective and less energy-intensive graphite for various applications. In this work, we report the effects of two-dimensional nanomaterials, graphene oxide (GO) and its derivative, reduced graphene oxide (RGO), used as templating agents for the graphitization of alkali-derived lignin. The hypothesis is that during heat temperature treatment, the GO additives act as a template that allows the lignin matrix to align on its basal planes through $\pi-\pi$ interactions. In addition, possible chemical bonding between the GO additives and lignin may extend the two planar frameworks. Results from X-ray diffraction and Raman spectroscopy showed improved graphitic quality in the lignin-GO and lignin-RGO samples compared to pure lignin at 2500 °C. Transmission electron microscopy images and selected area electron diffraction patterns also revealed ordered nanostructures and defined polycrystalline patterns in the lignin-GO and lignin-RGO samples. This work presents a method to synthesize graphitic-like materials using carbon-based templates with the advantage that there is no need for further purification of the final material as in the case of transition metal catalysts.

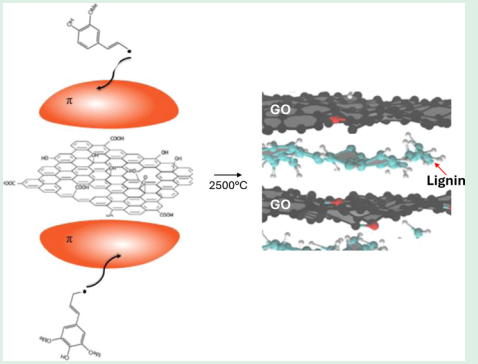

KEYWORDS: *lignin, graphene oxide (GO), reduced graphene oxide (RGO), templating, graphitization*

1.. INTRODUCTION

Lignin is the second most abundant natural polymer (derived from biomass) after cellulose.[1] It accounts for up to 30 wt % of wood.[2,3] It has been reported that over 130 million tons of waste lignin are produced in the paper making industry annually.[4] However, its use has been limited; most of it is burned to produce process heat or discharged into rivers causing serious environmental pollution.[5] Lignin possesses many remarkable properties such as high carbon content, good thermal stability, biocompatibility, degradability, etc.,[6,7] which makes it a great potential precursor for several industrial and commercial applications. These properties combined with lignin's low cost, abundance, and renewable origin have created the motivation and research interest in finding functional applications and converting lignin to high-value products.[8] Lignin-derived carbon materials (LDCMs) are being considered for batteries,[8,9] supercapacitors, carbon fibers,[6,10,11] catalysis, and environmental applications. Developing LDCMs for these applications would create a way to integrate renewable and sustainable materials for future energy demands and address environmental issues.[12,13]

However, it has been a challenge to graphitize LDCMs into high-value products or to use them as a precursor for carbon composite materials. This is because lignin is a non-graphitizable carbon, i.e., it does not go through a liquid crystalline state (mesophase stage) during carbonization due to its oxygen-rich backbone which facilitates cross-linking and curvature in its structure. This makes LDCMs equate to hard carbons that are difficult to graphitize after heat temperature treatment (HTT) which is in sharp contrast to the petroleum-based precursors (petroleum coke and pitch) that form highly graphitic materials after HTT.

Attempts have been made to design various methods to graphitize LDCMs. Johnson et al. heat-treated lignin-based carbon fibers at 1500 and 2000 °C to determine graphitic quality of the fibers. Characterization from X-ray diffraction (XRD) and high-resolution transmission electron microscopy (HRTEM) showed a poorly developed lattice structure and no preferred orientation at 1500 °C. The fibers heat-treated at 2000 °C also showed no preferred orientation but with some heterogeneity in the sample structure consisting of discontinuous and continuous inclusions of graphitic planes. This heterogeneity in the 2000 °C sample structures was attributed

Received: August 8, 2024
Revised: November 5, 2024
Accepted: November 9, 2024
Published: November 21, 2024

https://doi.org/10.1021/acsabm.4c01122
ACS Appl. Bio Mater. 2024, 7, 8319−8327

to the presence of impurities that may have caused catalytic graphitization. Another study showed inorganic impurities to improve the graphitic quality of kraft lignin derived from eucalyptus by heat treatment of samples up to 2800 °C (3073 K).[14] The samples used were initially washed with sulfuric acid and thermally treated to obtain different chars/ash content. After HTT of the medium ash char (0.17%) lignin sample up to 2800 °C, XRD and Raman showed progressive structural order as HTT increased, indicating improved graphitic quality of the lignin sample. This improvement was attributed to the presence of inorganic matter impurities present in the lignin based on its ash content.

Catalytic graphitization of kraft lignin to graphene-based structures using four different transitional metals (Ni, Cu, Fe, and Mo) has also been reported.[15] The main product after heat treatment at 1000 °C was multilayer graphene-encapsulated metal nanoparticles along with some graphene sheets/flakes. Raman spectra showed the presence of D and G bands, which suggested a low degree of graphitization, and it was found that the particle sizes and graphene shell layers were affected by the promoted metals.

Liu et al.[2] used alkali lignin as a carbon precursor to prepare carbon nanosheets (CNSs) by freeze-casting of a lignin aqueous dispersion and then direct carbonization at 900 °C. The CNSs were prepared from 5, 10, and 20 mg/mL lignin aqueous dispersions. The graphitic quality was measured using Raman analysis, wherein the lignin-derived nanofibers showed prominent D and G bands, indicating a low graphitic quality of the fibers. It was also found that the graphitic degree of CNSs decreased with increasing concentration of lignin precursor dispersion because thinner lignin sheets facilitate easier removal of volatile products during carbonization.

While the use of catalysts and the presence of impurities has been studied to accelerate or induce graphitization of LDCMs (with varied success and the need for purification of the resultant products), there is little work exploring the graphitization of lignin by templating using two-dimensional materials such as graphene oxide (GO). There is, however, research to suggest that templating by GO has the potential to aid graphitization of biomaterials. The use of GO as a templating agent has proven to be successful in the graphitization of biomaterials such as sugar.[16] It was shown that GO additives improved the graphitic quality of the sugar due to radical sites of the GO reactively bonding to the decomposing sugar matrix during HTT; this process was called chemical templating.[16] Another proposed factor that could contribute to improved graphitization is the interaction between the emerging aromatic domains within the matrix and the sp^2 framework of the GO, leading to alignment and orientation (physical templating). These results suggest that templating graphitization of lignin using GO is worth exploring. The same oxygen functional groups on GO that were key to sugar graphitization potentially could similarly graphitize lignin by reactive templating.

Furthermore, studies using molecular dynamics (MD) and reactive force field (ReaxFF) simulations have supported mechanisms of chemical reactiveness and physical templating. One such study by Rajabpour et al.,[17] MD and ReaxFF simulations showed the addition of graphene to the polyacrylonitrile (PAN) matrix improved alignment of 6-member carbon rings possibly due to $\pi-\pi$ interactions. Similarly, Papkov et al.[18] ran simulations using carbon nanotubes (CNTs) and graphene as templates in the PAN matrix and found improved alignment between the surface of the templates and the newly formed aromatic carbon during the carbonization process. Independent results from MD and ReaxFF simulations showed active sites for bonding were not found on the surface of the templates but instead on the edge sites where C−H bonds break and form radical sites for bonding with the PAN matrix. With these findings, it is possible that oxygen groups at the edge sites of GO templates could play a similar role in the bonding and alignment of the lignin matrix.

In this work, we report the effect of two-dimensional materials, GO and its derivative, RGO, as templating aids for the graphitization of lignin (alkali derived). The hypothesis is that these additives act as templates to graphitize lignin using $\pi-\pi$ interactions. In addition, possible chemical bonding between the GO additives and lignin may extend the two planar frameworks. It was found that lignin samples with either GO or RGO showed improved d(002) interplanar spacing, L_a (crystallite size), L_c (crystallite height) values compared to pure lignin when all samples were treated at 2500 °C. Raman spectra further confirmed the improved graphitization in lignin-GO and lignin-RGO by measuring less disorder in these materials compared to pure lignin. Furthermore, transmission electron microscopy images and selected area electron diffraction patterns revealed ordered nanostructures and defined polycrystalline patterns in the lignin-GO and lignin-RGO samples. This work presents a method to synthesize graphitic-like material using carbon-based templates, with the advantage that there is no need for further purification of the final material as in the case of transition metal catalysts.

2. EXPERIMENTAL METHODS

2.1. Materials and Preparation. Lignin, alkali, was obtained from Sigma-Aldrich (8068-05-1). The nanomaterial additives RGO and GO were obtained from Cheap Tubes. Lignin-RGO and lignin-GO were made using 2.5 wt % of each additive. The mixtures were sonicated in methanol for 15 min and left in the oven at 200 °C for 5 h.

Table 1. Chemical Composition of GO and RGO Additives Measured by XPS

sample	% additive carbon content	% additive oxygen content	minor elements in additive
RGO	81.9	14.4	N (3.7%)
GO	68.0	30.8	Si (0.6%) S (0.6%)

2.2. Carbonization. The three samples (lignin, lignin-GO, and lignin-RGO) were carbonized at 500 °C for 5 h in an inert atmosphere using a tubing bomb reactor.

2.3. Graphitization. The carbonized samples were graphitized at 1000, 1500, and 2500 °C. The 1000 °C graphitization was done in a Thermolyne 2110 tube furnace at 15 °C/min. The 1500 °C was done in a GSL-1700X-UL furnace at a 10 °C/min temperature ramp up to 900 °C and then 5 °C/min to 1500 °C. Graphitization was done at 2500 °C in a Centorr Vacuum Industries series 45 graphitization furnace, heating at 15 °C/min to 1000 °C, 10 °C/min to 2000 °C, and finally 5 °C/min to 2500 °C. All graphitization runs were performed under an Argon atmosphere.

2.4. Characterizations. *2.4.1. Fourier Transform Infrared Spectroscopy (FT-IR).* FT-IR was performed on a Bruker vertex 80 spectrometer. IR spectra were collected using the attenuated total reflected (ATR) method for the pure lignin and stabilized samples at 200 °C. Diffuse reflectance infrared Fourier transform spectroscopy (DRIFTS) was used to collect spectra for samples carbonized at 500 °C.

https://doi.org/10.1021/acsabm.4c01122
ACS Appl. Bio Mater. 2024, 7, 8319−8327

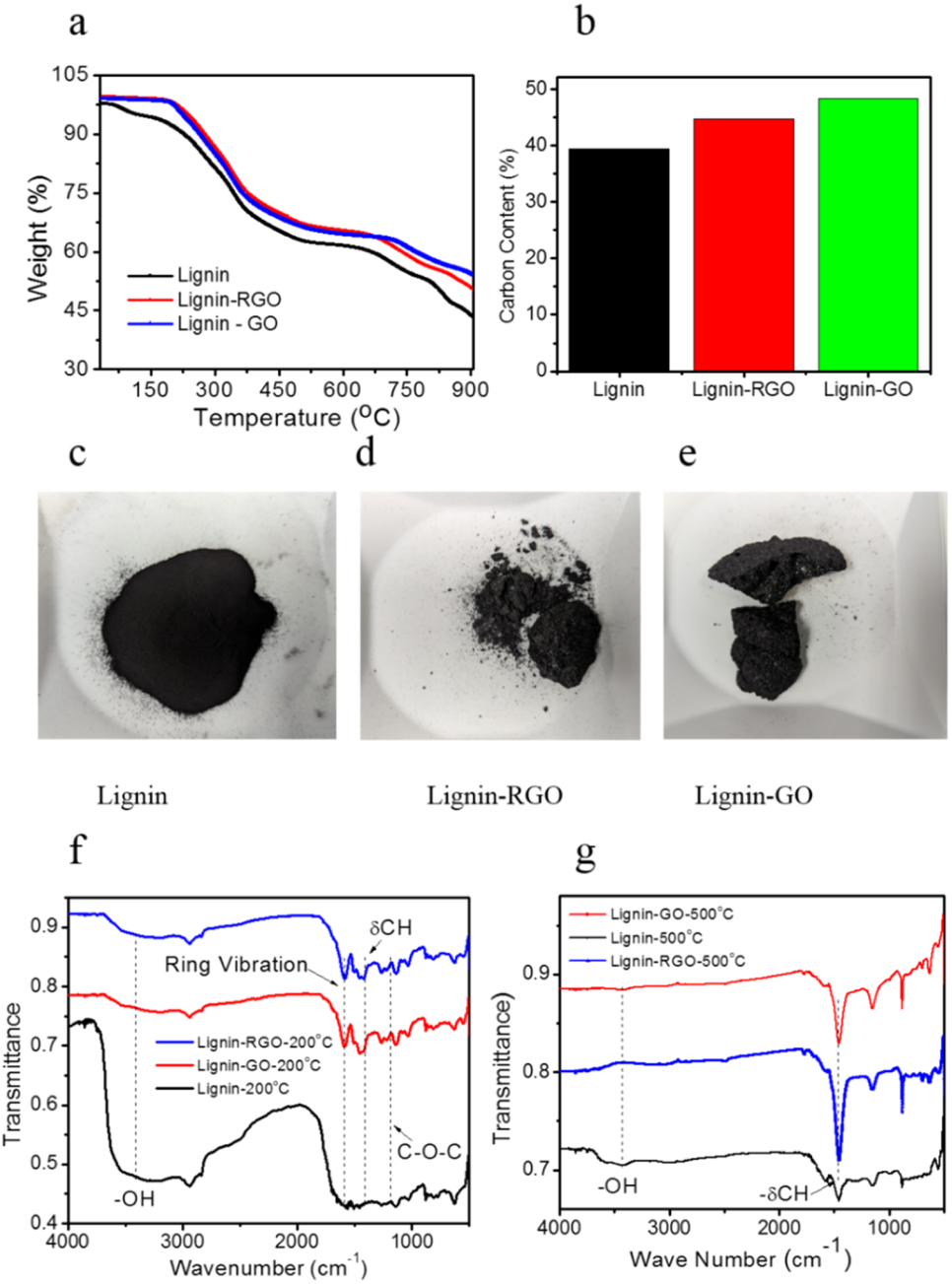

Figure 1. (a) TGA analysis of lignin, lignin-RGO, and lignin-GO. (b) Bar graph showing carbon content of lignin, lignin-RGO, and lignin-GO; images of samples after stabilization at 200 °C (c) lignin, (d) lignin-RGO, and (e) lignin-GO; FT-IR analysis of lignin, lignin-GO, and lignin-RGO after (f) stabilization at 200 °C and (g) carbonization at 500 °C.

2.4.2. Thermogravimetric Analysis (TGA). Thermogravimetric analysis (TGA) was done on a Q600 (TA Instruments). Samples (lignin, lignin-GO and lignin-RGO) were subjected to a temperature ramp test (30−900 °C at 10 °C/min).

2.4.3. X-ray Diffraction (XRD). The X-ray diffraction patterns were collected using a Malvern PANalytical Empyrean diffractometer equipped with a Cu source ($\lambda \cong 1.54$ Å), para-focusing optics, and a PIXcel 3D detector. The spectrum was scanned in the 2θ range of 10−90°. The background subtraction, peak fitting, and quantification were done using MDI JADE software.

2.4.4. Transmission Electron Microscopy (TEM) and Selected Area Electron Diffraction (SAED). Transmission electron microscopy samples were prepared by sonicating a few milligrams (mg) of the graphitized material in ethanol and then dropping it on a copper (Cu)-supported lacey carbon grid and allowed to dry. The samples were imaged using a FEI TalosTM F200X scanning/transmission electron microscope equipped with a FEG source providing 0.12 nm resolution. The instrument was operated at 200 kV and the samples were imaged at various magnifications in the ranges. SAED patterns were taken concurrently with TEM imaging.

2.4.5. Raman Spectroscopy. Raman spectra were collected using a Horiba LabRAM HR Evolution instrument equipped with 300 grooves/mm grating and a 532 nm laser. The spectra were acquired in DuoScan mode, which increases the statistical significance of the data by rastering over a wider area. At least 5 measurements were collected for each sample to make the analysis more representative.

2.4.6. Scanning Electron Microscopy (SEM). SEM images were taken with a field-emission SEM, an Apreo 5. Samples were prepared by placing a few milligrams on a carbon-taped pin stub holder. To obtain FESEM images, an acceleration voltage of 7 kV and a working distance between 11 and 7 mm was maintained.

https://doi.org/10.1021/acsabm.4c01122
ACS Appl. Bio Mater. 2024, 7, 8319−8327

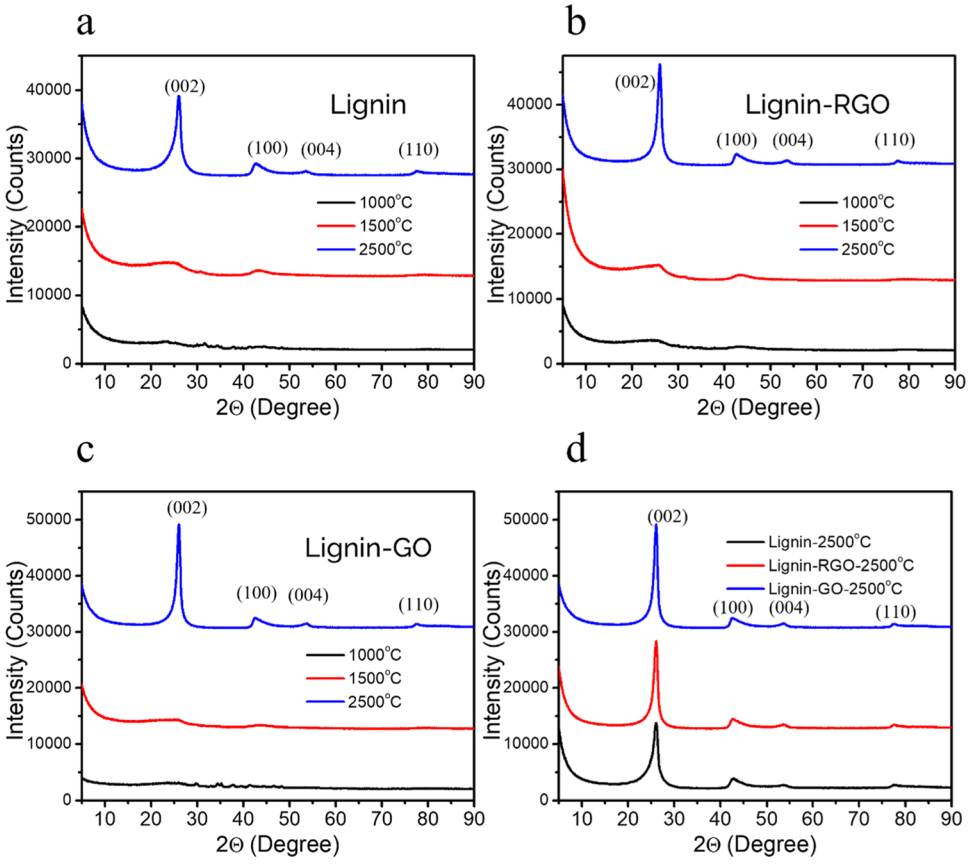

Figure 2. X-ray diffraction patterns across the temperature series: 1000 °C, 1500, and 2500 °C. (a) Lignin, (b) lignin-RGO, and (c) lignin-GO materials; (d) overlay of lignin, lignin-RGO, and lignin-GO carbons at 2500 °C.

2.4.7. X-ray Photoelectron Spectroscopy (XPS). XPS experiments were performed using a Physical Electronics VersaProbe II instrument equipped with a monochromatic Al K_α X-ray source ($h\nu$ = 1486.7 eV) and a concentric hemispherical analyzer. Charge neutralization was performed using both low energy electrons (<5 eV) and argon ions. The binding energy axis was calibrated using sputter cleaned Cu (Cu $2p_{3/2}$ = 932.62 eV, Cu $3p_{3/2}$ = 75.1 eV) and Au foils (Au $4f_{7/2}$ = 83.96 eV). Peaks were charged with reference to the C−C (sp^2) band in the carbon 1s spectra at 284.5 eV. Measurements were made at a takeoff angle of 45° with respect to the sample surface plane. This resulted in a typical sampling depth of 3−6 nm (95% of the signal originated from this depth or shallower). Quantification was done using instrumental relative sensitivity factors (RSFs) that account for the X-ray cross section and inelastic mean free path of the electrons (Table 1).

3. RESULTS AND DISCUSSION

The thermal degradation behavior of lignin, lignin-RGO, and lignin-GO samples after stabilization at 200 °C was evaluated using TGA (Figure 1). The temperature ramp was performed from room temperature to 900 °C followed by an isothermal hold for two h at 900 °C. At 100 °C, the thermogram of the pure lignin sample shows a weight loss of more than 5% compared to lignin-GO and -RGO samples, each with a loss of less than 1%. This is the temperature at which the absorbed water is lost. At 400 °C, the weight loss of lignin was 32%, compared to lignin-GO (29%) and lignin-RGO (28%) mixtures. The trend of more weight loss in lignin continues up to the final temperature 900 °C where lignin loses more than half its weight (57%), while for both lignin-GO and lignin-RGO, the corresponding weight losses were less than 50% (Figure 1).

Lignin is usually stabilized to increase carbon yield in carbon fiber production;[6,8,19] TGA analysis has shown higher carbon content in the lignin-GO and -RGO samples. It appears graphene oxide and reduced graphene oxide are stabilizing and/or cross-linking with lignin leading to the high carbon content observed. Physical evidence of cross-linking is also seen in (Figure 1c−e). At 200 °C, the lignin-GO and lignin-RGO samples formed solid structures at 200 °C unlike pure lignin, which remained in powder form.

To confirm the occurrence of cross-linking reactions, FT-IR was used to measure the changes in functional groups of lignin, lignin-GO, and lignin-RGO materials. Figure 1f shows the FT-IR spectra of the lignin, lignin-GO, and -RGO samples at 200 °C. The peak at ∼3300−3500 cm^{-1} can be attributed to the −OH group of lignin. It can be observed that −OH decreases with the addition of GO additives at 200 °C. This can be due to condensation or dehydration reactions between GO additives and lignin, causing loss of water leading to reduction in the −OH group. The peaks at 1591 and 1450 cm^{-1} appear to increase in lignin-GO and -RGO. These peaks are attributed to phenyl ring vibrations and a −CH stretch deformation, respectively.[20,21] Likewise, the peaks at 1338 and 1266 cm^{-1} are attributed to the C−O−C vibration increase, consistent with etheric bridge formation. These changes suggest an interaction between lignin and GO additives at 200 °C causing a loss of −OH, possibly in the form of water, and formation of new bonds such as C−O−C at ∼1200 cm^{-1}. This could explain the solidification of the lignin-GO and lignin-RGO

https://doi.org/10.1021/acsabm.4c01122
ACS Appl. Bio Mater. 2024, 7, 8319−8327

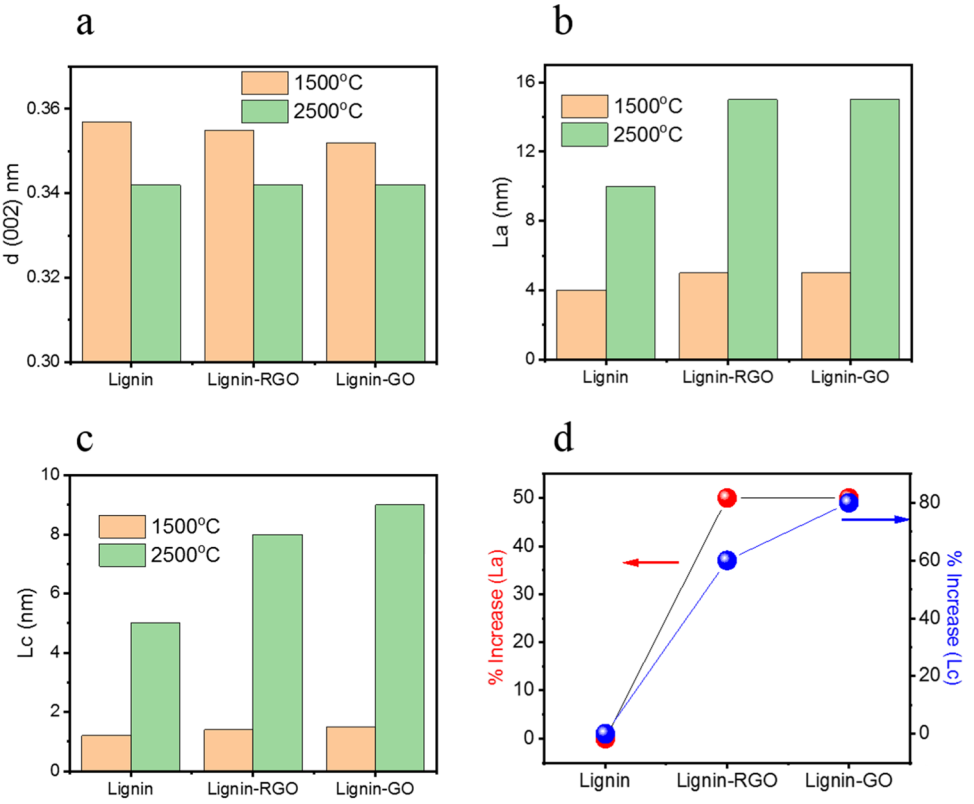

Figure 3. Lattice parameters extracted from deconvoluted XRD spectra of lignin, lignin-RGO, and lignin-GO. Bar graph showing changes in (a) d(002) values at 1500 °C and 2500 °C, (b) L_a values at 1500 °C and 2500 °C, and (c) L_c values at 1500 °C and 2500 °C; (d) % increase of L_a and L_c at 2500 °C.

samples. At 500 °C, a complete reduction in the −OH group at 3300 cm^{-1}, an increase at 1458 cm^{-1} peak, and enhancement of peaks around 900 and 800 cm^{-1} are observed for lignin-GO and lignin-RGO compared to pure lignin. After carbonization heat-treatment, it is expected that oxygen functional groups decrease and are lost in the form of CO and CO_2. Furthermore, the improved 1458 cm^{-1} peak can be attributed to the improvement of the alkyl stretch, $-CH_2$ symmetric scissoring. This is a sharp contrast to the eliminated C−H stretching between 2850 and 2950 cm^{-1}. This dichotomy is due to the origin of C−H stretching. The C−H stretching between 2850 and 2950 cm^{-1} originated from aliphatic methylene groups[22] which are easily lost or broken during carbonization heat-treatment and as a result, do not appear on the FT-IR spectra. However, C−H stretching at 1458 cm^{-1} is because of an aromatic ring vibration/stretching which increased from cyclization, dehydrogenation, and aromatization reactions occur during carbonization. Similarly, peaks between 900 and 750 cm^{-1} are attributed to C−H bending of aromatic ring.[22,23] This improvement is seen mostly in the lignin-GO and lignin-RGO from an increase in aromaticity after carbonization heat treatment. This indicates improved bonding between lignin and GO additives.

X-ray diffraction (XRD) is a primary technique used to determine the crystallinity of materials. Figure 2a shows the XRD spectra of lignin at different HTTs. There is no sign of graphitic-like materials (low crystallinity/amorphous quality) observed for lignin at 1000 °C and 1500 °C indicated by the low intensity and very broad d(002) peak as well as undefined peaks at higher angles. However, there is improved crystallinity at HTT of 2500 °C indicated by the higher intensity and narrower d(002) peak, and better-defined higher angle peaks of d(100) at 43° and d(110) at 78°. The d(002) peak of lignin at 2500 °C does not resemble that of graphite which is very intense and sharp. The improved crystallinity of lignin can be attributed to small crystallites which formed at 2500 °C but their formation does not signify long-range order.

The same trend is observed in lignin-GO and -RGO samples at the lower HTT of 1000 °C and 1500 °C (Figure 2b,c). There is no observed graphitization, as indicated by the low intensity and broad d(002) peak. However, at HTT of 2500 °C, both samples, lignin-GO and -RGO, show improved crystallinity (less amorphous phase) shown by the higher intensity and narrower d(002) peak. The higher angle peaks, d(100), d(101), and d(110) at 43, 54, and 78°, respectively, are also better defined. Figure 2d depicts the spectra of lignin, lignin-RGO, and lignin-GO at 2500 °C. The d(002) peak of pure lignin is broader especially in the lower angle regions compared to the narrower and sharper peaks of lignin-RGO and lignin-GO. The presence of the GO and RGO appears to improve the graphitization of pure lignin but only at a high heat treatment temperature (2500 °C). This is further confirmed with XRD lattice parameters (d(002), L_a, and L_c) and subsequent characterization techniques.

Figure 3 plots the XRD lattice parameters of lignin, lignin-GO, and lignin-RGO. Three XRD parameters are typically used to measure graphitization: interlayer spacing (d(002)), crystallite size (L_a), and crystallite height (L_c). The d(002) is a primary measure of graphitization, and a decrease in d(002) implies a higher degree of graphitization (improved graphitic quality). The d(002) peak was deconvoluted into two phases, the amorphous and crystalline phases, due to its broadness and

https://doi.org/10.1021/acsabm.4c01122
ACS Appl. Bio Mater. 2024, 7, 8319−8327

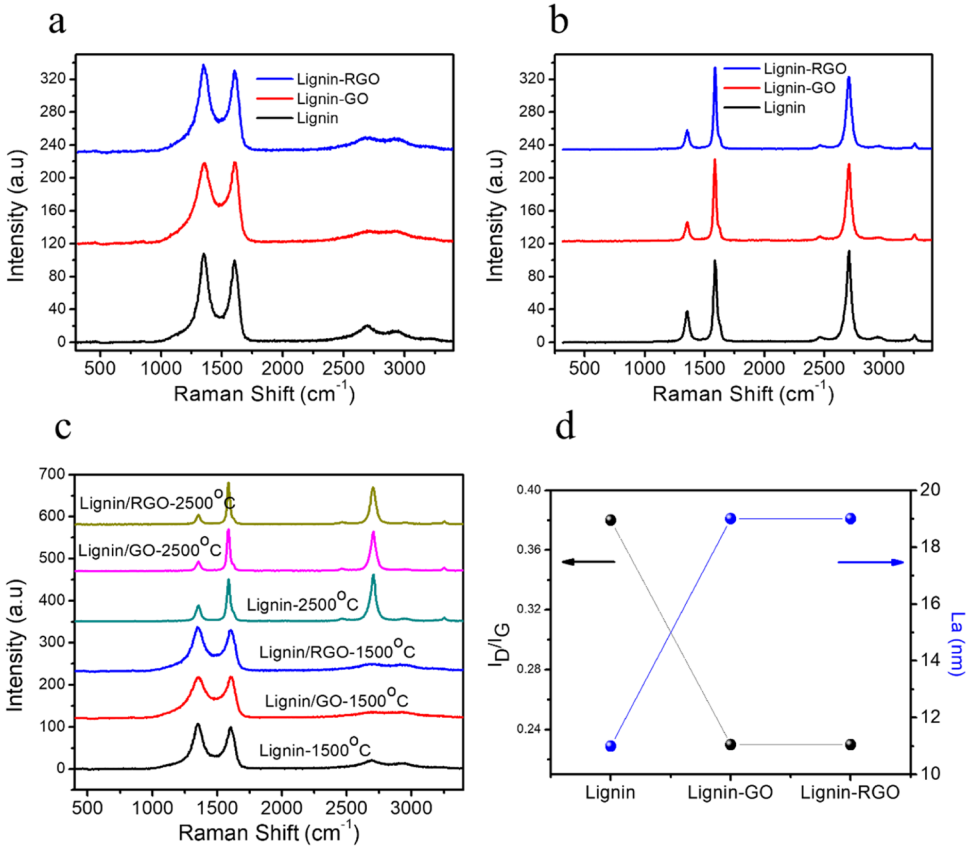

Figure 4. Raman Spectroscopy analysis of lignin, lignin-RGO, and lignin-GO (a) graphitized at 1500 °C, (b) graphitized at 2500 °C; (c) overlay of 1500 °C and 2500 °C spectra and (d) I_D/I_G and L_a values extracted at 2500 °C.

Table 2. Raman Analysis of Lignin, Lignin-GO, and Lignin-RGO

samples	I_D/I_G	G-peak position (cm^{-1})	G_{fwhm}	I_{2D}/I_G	$2D_{fwhm}/G_{fwhm}$	D_{fwhm}/G_{fwhm}
lignin	0.38	1588	32.5	1.09	1.52	1.37
lignin-GO	0.22	1586	26.2	0.92	1.82	1.58
lignin-RGO	0.22	1587	24.8	0.89	1.87	1.58

asymmetry. Also, an increase in the L_a and L_c values signifies an increase in graphitic quality. In Figure 3a, the bar graph shows a decrease of d(002) values from 1500 °C to 2500 °C. This is true for lignin, lignin-GO, and lignin-RGO and signifies an improvement in graphitic quality in all samples from 1500 °C to 2500 °C. Lignin, lignin-GO, and lignin-RGO have equal d(002) values (0.342 nm) at 2500 °C. In addition, there is a rise in L_a and L_c values when the samples are heated to 2500 °C (Figure 3b,3c), and there is a significant increase of L_a and L_c for the lignin-RGO and lignin-GO compared to pure lignin at 2500 °C. At 2500 °C, lignin-GO and lignin-RGO have equal L_a values of 15 nm compared to pure lignin with L_a of 10 nm. Likewise, the L_c values for lignin-GO and lignin-RGO are 9 and 8 nm, respectively, compared to that for pure lignin (5 nm). The larger crystallite parameters indicate a greater degree of graphitization (or improved graphitic quality) for lignin-RGO and lignin-GO. The L_a and L_c trends at 2500 °C are clearly depicted in the line graph in Figure 3d. Overall, there was a 50% increase in L_a for both lignin-GO and lignin-RGO compared to pure lignin. Also, there is an 80% increase in L_c for lignin-GO and a 60% increase in the L_c for lignin-RGO compared to pure lignin. The increases in L_a and L_c are attributed to the templating effect of the graphene oxides on lignin.

Raman spectroscopy is another important technique for characterizing the graphitic quality of carbon materials. The G-peak at 1580 cm^{-1} is characteristic of sp^2 hybrid structure, which represents the symmetry and crystallinity of graphene materials; the D-peak at 1350 cm^{-1} is a defect peak, representing the defects and disorder of graphite layers.[24,25] Figure 4a shows the Raman spectra of the lignin, lignin-GO, and lignin-RGO samples graphitized at 1500 °C. It can be observed that the D-peak of all samples is prominent and broad in all of the samples. This suggests poor graphitic quality of the samples at 1500 °C and shows that 1500 °C is too low a temperature to remove defects, enable sheet stacking and thus improve graphitic quality of the lignin, lignin-GO, and lignin-RGO composites. The opposite is true for the samples graphitized at 2500 °C (Figure 4b). At this high-temperature treatment, there is an observable increased crystallinity, i.e., graphitization degree, for all lignin samples (lignin, lignin-GO, and lignin-RGO) as seen by the low D-band intensity and narrower and intense G-band at around 1580 cm^{-1}. With graphene oxide additives (Figure 4b,c), there are fewer defects (and improved graphitization), attributed to the templating effect of the graphene oxide. Figure 4c shows the Raman spectra for all lignin samples as the HTT increases. A progression in graphitic crystallinity is clearly seen in all

https://doi.org/10.1021/acsabm.4c01122
ACS Appl. Bio Mater. 2024, 7, 8319−8327

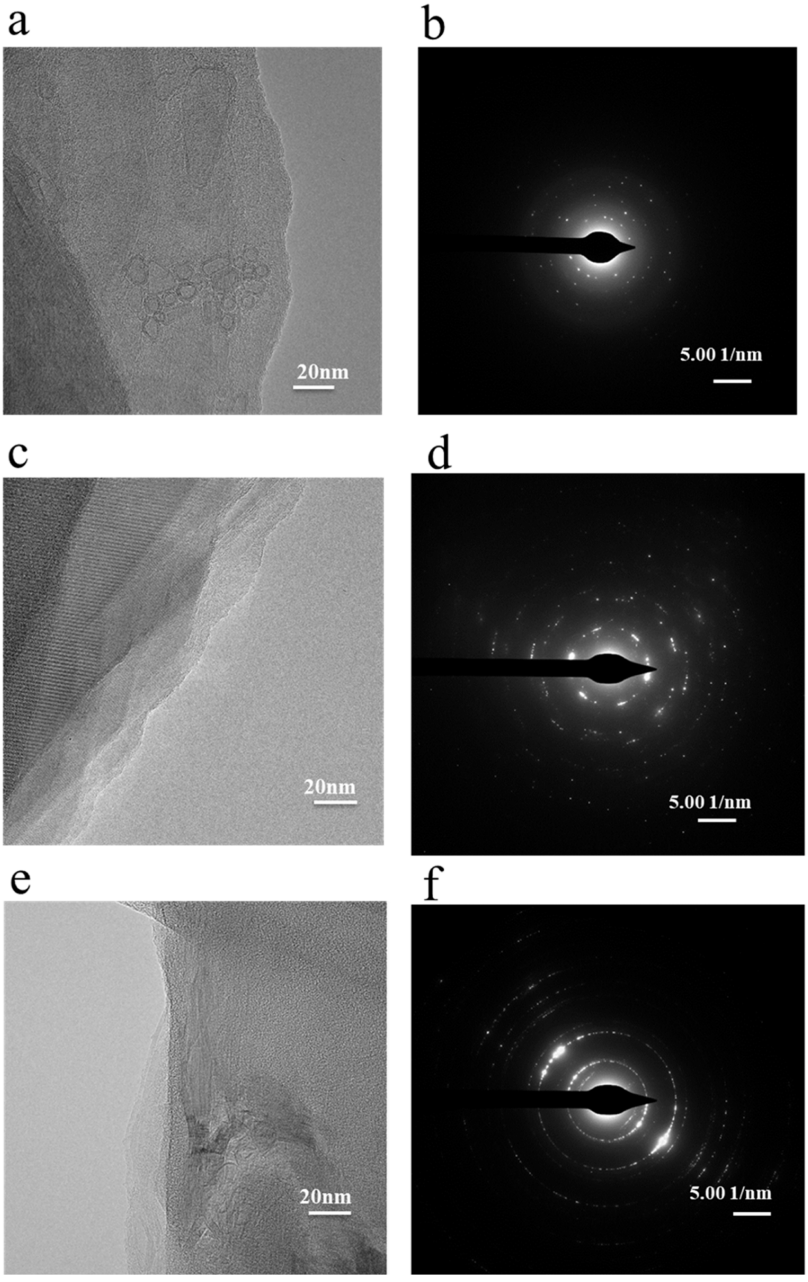

Figure 5. Transmission electron microscopy and selected area diffraction patterns of (a, b) lignin, (c, d) lignin-RGO, and (e, f) lignin-GO composites.

samples as HTT increases. Lignin-RGO and lignin-GO samples appear with less defects and disorder (low-band intensity) and higher graphitic quality as the temperature increased to 2500 °C. The results from Raman analysis support results extracted from the XRD spectra. This is further confirmed in Figure 4d which shows the I_D/I_G and L_a values for lignin, lignin-GO, and lignin-RGO graphitized at 2500 °C. A decrease in I_D/I_G corresponds to an increased graphitic carbon content. Pure lignin has the highest I_D/I_G ratio (0.38) and lowest L_a (11 nm) value, indicating that it is the least graphitized sample. Meanwhile I_D/I_G decreases (0.22) and L_a increases (19 nm) for lignin-RGO and lignin-GO materials, which indicates an increase in graphitic quality (improved graphitization). It is important to note that lignin-RGO and lignin-GO have equivalent I_D/I_G and L_a values. This confirms the XRD results, wherein the lignin-GO and lignin-RGO samples exhibited similar graphitic quality.

A more in-depth Raman analysis reveals distinctions between pure lignin and the lignin -GO, -RGO samples, as illustrated in Table 2. The initial column presents the intensity ratio of the D to G band (I_D/I_G), a metric reflecting the defect and disorder levels in samples. Decreasing I_D/I_G values correspond to a heightened graphitic carbon content. Lignin-GO and lignin_RGO exhibit equivalent low I_D/I_G values of 0.22, indicative of low disorder and high graphitic quality. Conversely, pure lignin exhibits a higher I_D/I_G ratio (0.38), suggesting increased defect levels and a diminished graphitic quality. The subsequent columns detail the G-peak position, and the G-full width half-maximum (G-fwhm) provide clear evidence of the disparity in crystalline content between pure lignin and GO additive samples. The smaller, narrower G-

https://doi.org/10.1021/acsabm.4c01122
ACS Appl. Bio Mater. 2024, 7, 8319−8327

fwhm signifies higher graphitic quality. Lignin-GO and lignin-RGO exhibit lower G-fwhm values than pure lignin.

Further analysis of Raman parameters, including the ratio of the 2D to G band (I_{2D}/I_G), underscores improved graphitic layers in lignin-GO and lignin-RGO samples, as they exhibit lower I_{2D}/I_G values. This trend is also observed in the fwhm ratio of the 2D to G and D to G band in the last two columns, with higher values for lignin-GO and lignin-RGO compared to pure lignin. These findings suggest lower defects and enhanced crystalline content in the lignin-GO and lignin-RGO sample. It appears that the addition of GO-derived additives into the lignin matrix can influence the formation of larger crystallites and improve the overall structure.

Figure 5 shows the TEM images and SAED patterns for lignin (a, b), lignin-GO (c, d), and lignin-RGO (e, f) carbons. The TEM image of lignin (Figure 5a) shows a disordered nanostructure indicative of a nongraphitizing matrix. Curved structures yet embedded also support disorder in the nanostructure. The SAED pattern of lignin (Figure 5b) shows the presence of nanocrystallites (which arose from the HTT at 2500 °C) but does not imply long-range order in the pure lignin sample. However, the TEM images of lignin-RGO (Figure 5c) and lignin-GO (Figure 5e) show an improved nanostructure with sheet stacking and the presence of lattice fringes indicative of a graphitizing matrix. This suggests a templating interaction between the graphene oxide additives and lignin matrix led to a change in the nanostructure and hence graphitic quality of the matrix. Furthermore, the SAED images of lignin-RGO (Figure 5d) and lignin-GO (Figure 5f) show improved polycrystalline patterns, supporting evidence of improved graphitic quality of the lignin precursor caused by the addition of the GO additives. It is evident that the graphene oxide additives are templating the lignin matrix causing it to change from a nongraphitizing precursor into a graphitizing one. These observations are consistent with results from deconvoluted XRD and Raman.

4. CONCLUSIONS—THE EFFECT OF CHEMICAL AND PHYSICAL TEMPLATING

The hypothesis for this work is that graphene oxide additives can induce graphitization of the lignin matrix by the process of templating during heat treatment. Characterization by XRD showed improvement in the graphitic quality (measured by lattice parameters, crystallite height, and size) in lignin-GO and lignin-RGO. There was an overall 50% increase in crystallite size, L_a, and between a 60% and 80% increase in crystallite height, L_c, for lignin-RGO and lignin-GO compared to pure lignin. This improvement in graphitic quality was supported by Raman analysis, which revealed lower disorder in these lignin-GO and -RGO materials compared to pure lignin. Furthermore, TEM images and SAED patterns showed orderliness in the nanostructure with presence of lattice fringes, sheet stacking and sharp and defined polycrystalline patterns. All this evidence points to an increase in the graphitic quality facilitated by the addition of GO and RGO two-dimensional (2D) templates. Graphene oxides are well-known for their two-dimensional sp^2 framework which can serve as "confinement" for directing the structure of housing matrix. We propose this as the operative feature by which the GO additive directs the nano- to microstructure of the lignin matrix. With the extended sp^2 framework, the GO and RGO act as a "template" to guide graphitic development by process of $\pi-\pi$ interactions. This appears as the major driving force of graphitization. Considering that the presence of oxygen groups on the graphene layer creates a mixed sp^2-sp^3 state, however, there is still a large portion (between 40% and 60%) which are unfunctionalized and provides the sp^2 framework for templating the lignin matrix into graphitic materials. Moreover, during heat treatment, the defunctionalization of the GO and RGO additives extends the sp^2 framework and further guides the templating of lignin. In addition, possible chemical bonding between the GO additives and lignin may extend the two planar frameworks.

Related ReaxFF molecular dynamics simulations also support templating mechanisms of the GO-derived additives.[26] Mechanisms depicted by Gharpure et al.[26] are similar to observations and trends seen in the above experimental results of lignin-GO and lignin-RGO. It can therefore be surmised that GO additives act as templating agents resulting in the change in structure and properties of lignin. The use of the 2D carbon-based additives in the form of graphene oxide as a "template graphitization agent" is a novel process in transforming the structure of bio precursors such as lignin. This technique provides the advantage of no further purification of the final material, as in the case of transition metal catalysts.

AUTHOR INFORMATION

Corresponding Author

Sandra N. Ike − *The John and Willie Leone Family Department of Energy and Mineral Engineering, The Pennsylvania State University, State College, Pennsylvania 16801, United States; EMS Energy Institute, The Pennsylvania State University, State College, Pennsylvania 16801, United States;* orcid.org/0009-0007-7436-8691; Email: sxi5097@psu.edu

Author

Randy L. Vander Wal − *The John and Willie Leone Family Department of Energy and Mineral Engineering, The Pennsylvania State University, State College, Pennsylvania 16801, United States; EMS Energy Institute, The Pennsylvania State University, State College, Pennsylvania 16801, United States;* orcid.org/0000-0002-5847-9726

Complete contact information is available at: https://pubs.acs.org/10.1021/acsabm.4c01122

Notes

The authors declare no competing financial interest.

ACKNOWLEDGMENTS

This material is based upon work supported by the U.S. National Science Foundation under award No. 2306042.

REFERENCES

(1) Ge, Y.; Li, Z. Application of Lignin and Its Derivatives in Adsorption of Heavy Metal Ions in Water: A Review. *ACS Sustainable Chem. Eng.* **2018**, *6*, 7181−7192.

(2) Liu, W.; Lu, X. Lignin-derived carbon nanosheets for high-capacitance supercapacitors. *RSC Adv.* **2017**, *7*, 48537−48543.

(3) Sen, S.; Sadeghifar, H.; Argyropoulos, D. S. Kraft Lignin Chain Extension Chemistry via Propargylation, Oxidative Coupling, and Claisen Rearrangement. *Biomacromolecules* **2013**, *14*, 3399−3408.

(4) Tribot, A.; Amer, G.; Abdou Alio, M.; et al. Wood-lignin : Supply, extraction processes and use as bio-based material. *Eur. Polym. J.* **2019**, *112*, 228−240.

(5) Xiao, X.; Jiang, C.; Zhang, Y.; Cai, Z.; Yu, P. Preparation and characterization of formaldehyde-modified black liquor lignin/poly

(propylene carbonate) composites. *Int. J. Polym. Anal. Charact.* **2018**, *23*, 346−353.
(6) Aslanzadeh, S.; Ahvazi, B.; Boluk, Y.; Ayranci, C. Carbon Fiber Production from Electrospun Sulfur Free Softwood Lignin Precursors. *J. Eng. Fibers Fabr.* **2017**, *12*, No. 155892501701200405, DOI: 10.1177/155892501701200405.
(7) Jiang, C.; Bo, J.; Xiao, X.; et al. Converting waste lignin into nano-biochar as a renewable substitute of carbon black for reinforcing styrene-butadiene rubber. *Waste Manage.* **2020**, *102*, 732−742.
(8) Zhang, W.; Qiu, X.; Wang, C.; et al. Lignin derived carbon materials : current status and future trends. *Carbon Res.* **2022**, *1*, 1−39.
(9) Talabi, S. I.; Luz, A. P. d.; Pandolfelli, V. C.; et al. Graphitization of lignin-phenol-formaldehyde resins. *Mater. Res.* **2020**, *23*, No. e20190686, DOI: 10.1590/1980-5373-mr-2019-0686.
(10) Misra, M. Processing, Carbonization, and Characterization of Lignin Based Electrospun Carbon Fibers. *Front. Energy Res.* **2020**, *8*, No. 00208, DOI: 10.3389/fenrg.2020.00208.
(11) Johnson, D. J. The Fine Structure OF Lignin-Based Carbon Fibers. *Carbon* **1975**, *13*, 321−325.
(12) Himmel, M. E.; Ding, S.; Johnson, D. K.; Adney, W. S.; et al. Biomass Recalcitrance : Engineering Plants and Enzymes for Biofuels Production. *Science* **2007**, *315*, 804−807.
(13) Wang, Z.; Shen, D. State-of-the-art on the production and application. *Green Chem.* **2018**, *20*, 5031−5057.
(14) Rodríguez-Mirasol, J.; Cordero, T.; Cordero, T.; Rodriguez, J. J. High-Temperature Carbons from Kraft Lignin. *Carbon* **1996**, *34*, 43−52.
(15) Yan, Q.; Li, J.; Zhang, X.; et al. Catalytic graphitization of kraft lignin to graphene-based structures with four different transitional metals. *J. Nanopart. Res.* **2018**, *20*, 223.
(16) Singh, M.; Vander Wal, R. L. Carbon Composites—Graphene-Oxide-Catalyzed Sugar Graphitization. *J. Carbon Res.* **2022**, *8*, 15.
(17) Rajabpour, S. et al. Polyacrylonitrile/Graphene Nanocomposite: Towards the Next Generation of Carbon Fibers. 2020, arXiv:2006.11985. arXiv.org e-Print archive. http://arxiv.org/abs/2006.11985.
(18) Papkov, D.; Goponenko, A.; Compton, O. C.; et al. Improved graphitic structure of continuous carbon nanofibers via graphene oxide templating. *Adv. Funct. Mater.* **2013**, *23*, 5763−5770.
(19) Correa, C. R.; Kruse, A. Biobased functional carbon materials: Production, characterization, and applications-A review. *Materials* **2018**, *11*, No. 1568, DOI: 10.3390/ma11091568.
(20) Kong, Y.; Wang, L.; Ge, Y.; Su, H.; Li, Z. Lignin xanthate resin-bentonite clay composite as a highly effective and low-cost adsorbent for the removal of doxycycline hydrochloride antibiotic and mercury ions in water. *J. Hazard. Mater.* **2019**, *368*, 33−41.
(21) Wang, S.; Hu, Z.; Shi, J.; et al. Green synthesis of graphene with the assistance of modified lignin and its application in anticorrosive waterborne epoxy coatings. *Appl. Surf. Sci.* **2019**, *484*, 759−770.
(22) Boeriu, C. G.; Bravo, D.; Gosselink, R. J. A.; Van Dam, J. E. G. Characterisation of structure-dependent functional properties of lignin with infrared spectroscopy. *Ind. Crops Prod.* **2004**, *20*, 205−218.
(23) Sammons, R. J.; Harper, D. P.; Labbé, N.; et al. Characterization of organosolv lignins using thermal and FT-IR spectroscopic analysis. *BioResources* **2013**, *8*, 2752−2767.
(24) Kudin, K. N.; Ozbas, B.; Schniepp, H. C.; et al. Raman spectra of graphite oxide and functionalized graphene sheets. *Nano Lett.* **2008**, *8*, 36−41.
(25) Dikin, D. A.; Stankovich, S.; Zimney, E. J.; et al. Preparation and characterization of graphene oxide paper. *Nature* **2007**, *448*, 457−460.
(26) Gharpure, A.; Kowalik, M.; Vander Wal, R. L.; van Duin, A. C. T. Upcycling Plastic Waste into Graphite Using Graphenic Additives for Energy Storage: Yield, Graphitic Quality, and Interaction Mechanisms via Experimentation and Molecular Dynamics. *ACS Sustainable Chem. Eng.* **2024**, *12*, 4565−4575.

https://doi.org/10.1021/acsabm.4c01122
ACS Appl. Bio Mater. 2024, 7, 8319−8327